Supporting Information

Atomic-Level Customization of Zinc Crystallization Kinetics at the Interface for High-Utilization Zn Anodes

Qin Liu[1], Xiong Liu[3], Yu Liu[1], Meng Huang[1], Weihao Wang[1], Yu Cheng[1], Hong Zhang[1] and Lin Xu[1,2*]

[1] State Key Laboratory of Advanced Technology for Materials Synthesis and Processing, Wuhan University of Technology, Wuhan, 430074, P. R. China

[*]E-mail: linxu@whut.edu.cn

ORCID: 0000-0003-2347-288X

[2] Hubei Longzhong Laboratory, Wuhan University of Technology (Xiangyang Demonstration Zone), Xiangyang, 441000, P. R. China

[3] School of Materials Science and Engineering, Zhengzhou University, Zhengzhou, 450001, P. R. China

Table S1. Number of ions and molecules, the total number of atoms and the size of simulation box for two modelling systems.

	No. of Zn^{2+}	No. of SO_4^{2-}	No. of La^{3+}	No. of Cl^-	No. of H_2O	Total no. of atoms	Simulation box size
2.0 M $ZnSO_4$	200	200	0	0	5500	17700	$(5.4256nm)^3$
0.3 M $LaCl_3$ 2.0 M $ZnSO_4$	200	200	30	90	5500	17820	$(5.4707nm)^3$

Table S2 The comparison of DOD and cumulative capacity with other reported literatures.

No.	Modified Strategy	DOD (%)	Cumulative capacity (mAh)	Current density*Areal capacity (mA cm^{-2}*mAh cm^{-2})
This work	**$ZnSO_4$-CFTA-H_2O**	**85.4**	**12000**	**800**
1	Zn/ZBO	60	12500	500
2	Self-adaptive EDL	85	3500	200
3	Zn/ZSO	1.7	7500	5
4	PEGTE-5	17	13000	100
5	Zn/NTP	57	2000	200
6	ZSM-5	1.7	2000	1
7	α-CD	30	1000	25
8	SL	80	2400	576
9	BET	3.4	1600	4
10	Zn@ZCO	42.5	5000	0.25
11	Zn/SHn	8.5	10000	50
12	MeOH	4.25	4500	6.25

Table S3 The specific number of different solvation structures of La^{3+} in a mixed solution of 2M $ZnSO_4$ and 0.3M $LaCl_3$, when the solvation structure contains zero Cl^-.

Cl=0	O_S=0	O_S=1	O_S=2	O_S=3	O_S=4
Ow=4	0.000	0.327	7.171	0.000	0.000
Ow=5	0.000	0.480	2.156	3.320	0.002
Ow=6	6.672	0.760	0.180	3.112	0.000
Ow=7	7.793	0.223	3.153	0.000	0.000
Ow=8	12.404	0.182	6.485	0.000	0.000
Ow=9	7.864	0.000	0.000	0.000	0.000
Ow=10	24.125	0.000	0.000	0.000	0.000

Table S4 The specific number of different solvation structures of La^{3+} in a mixed solution of 2M $ZnSO_4$ and 0.3M $LaCl_3$, when the solvation structure contains one Cl^-.

Cl=1	O_S=0
O_W=6	0.142
O_W=7	6.585
O_W=8	3.112
O_W=9	0.423

Table S5 The specific number of different solvation structures of La^{3+} in a mixed solution of 2M $ZnSO_4$ and 0.3M $LaCl_3$, when the solvation structure contains two Cl^-.

Cl=2	O_S=0
O_W=7	3.302
O_W=8	0.030

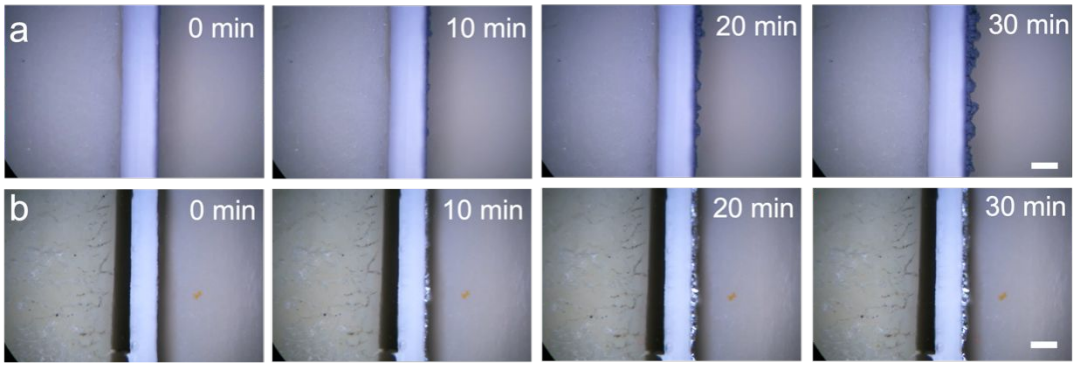

Figure S1. In situ optical microscope images of Zn deposition on the negative side in Zn||Zn symmetric systems: a) $ZnSO_4$-H_2O and b) $ZnSO_4$-CFTA-H_2O. Scale bar: 100 μm.

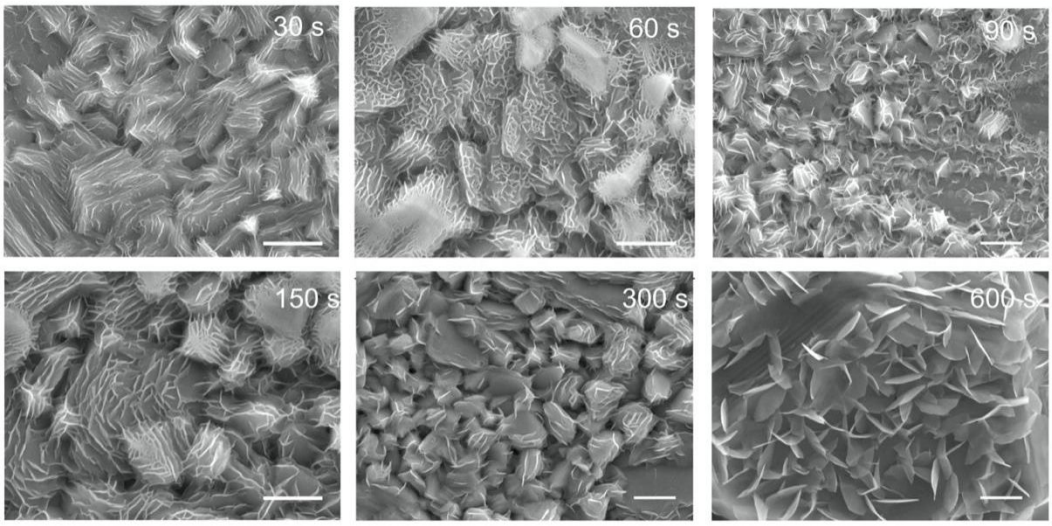

Figure S2. Ex-situ SEM characterization of Zn crystal growth behavior in $ZnSO_4$-H_2O systems at 5 mA cm^{-2}. Scale bar: 1 μm.

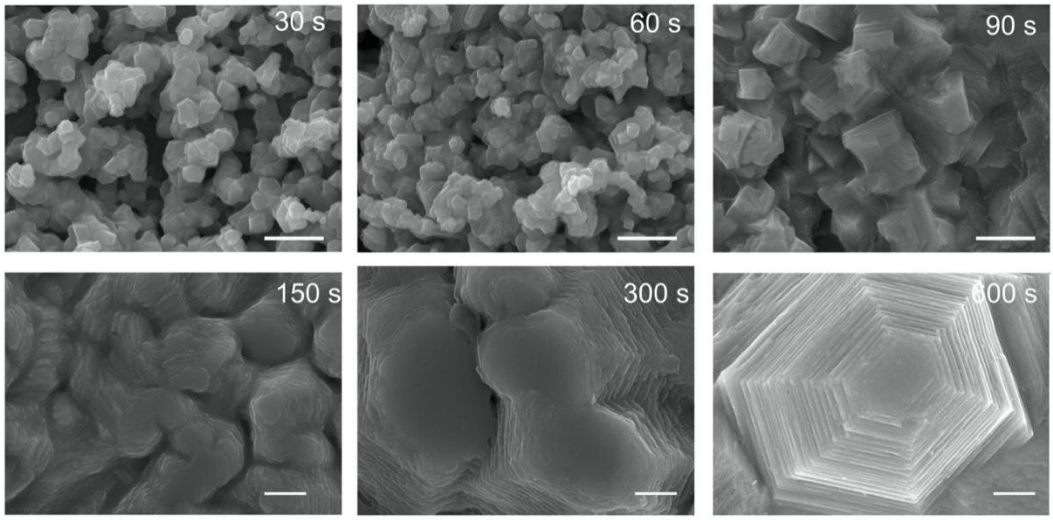

Figure S3. Ex-situ SEM characterization of Zn crystal growth behavior in $ZnSO_4$-CFTA-H_2O systems at 5 mA cm^{-2}. Scale bar: 1 μm.

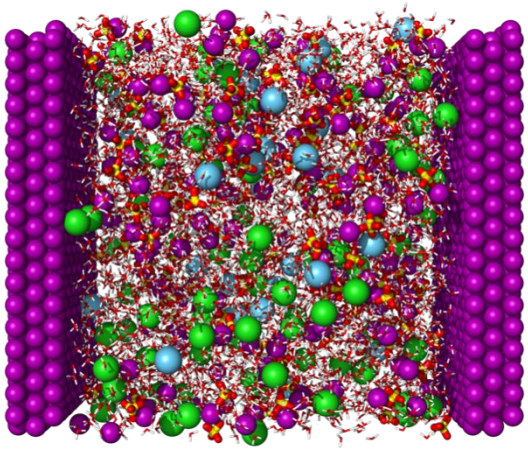

Figure S4. Visual representation of electrolyte species and simulation box for $ZnSO_4$-CFTA-H_2O electrolyte confined by two Zn electrodes.

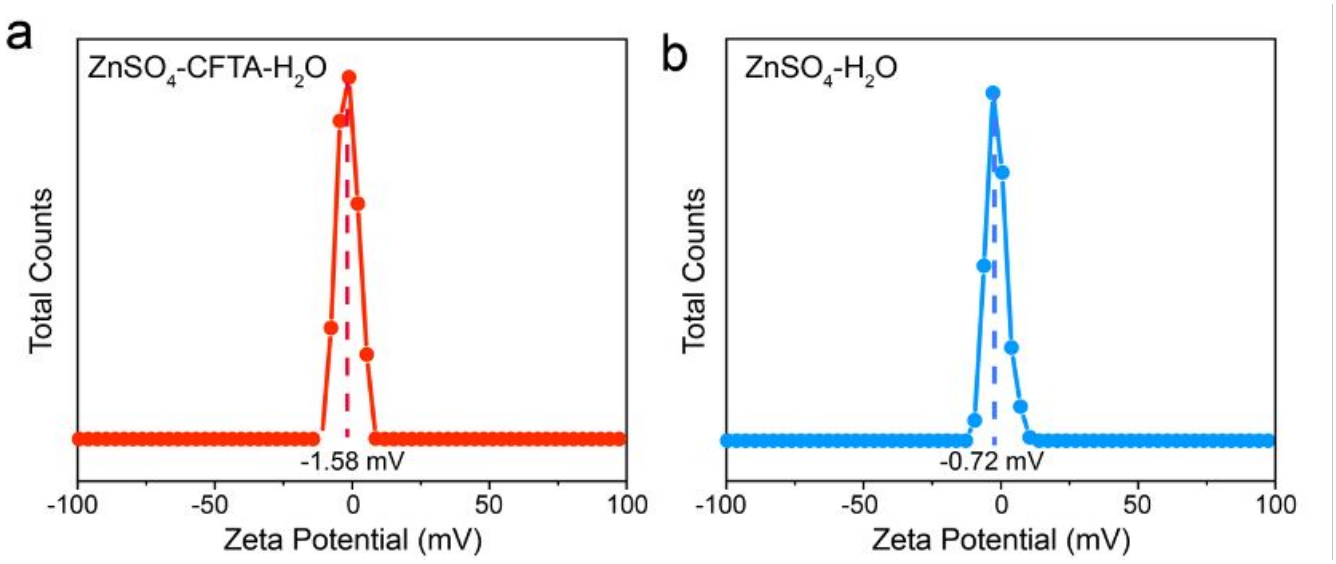

Figure S5. a) Zeta potential of Zn powder in $ZnSO_4$-CFTA-H_2O. b) Zeta potential of Zn powder in $ZnSO_4$-H_2O.

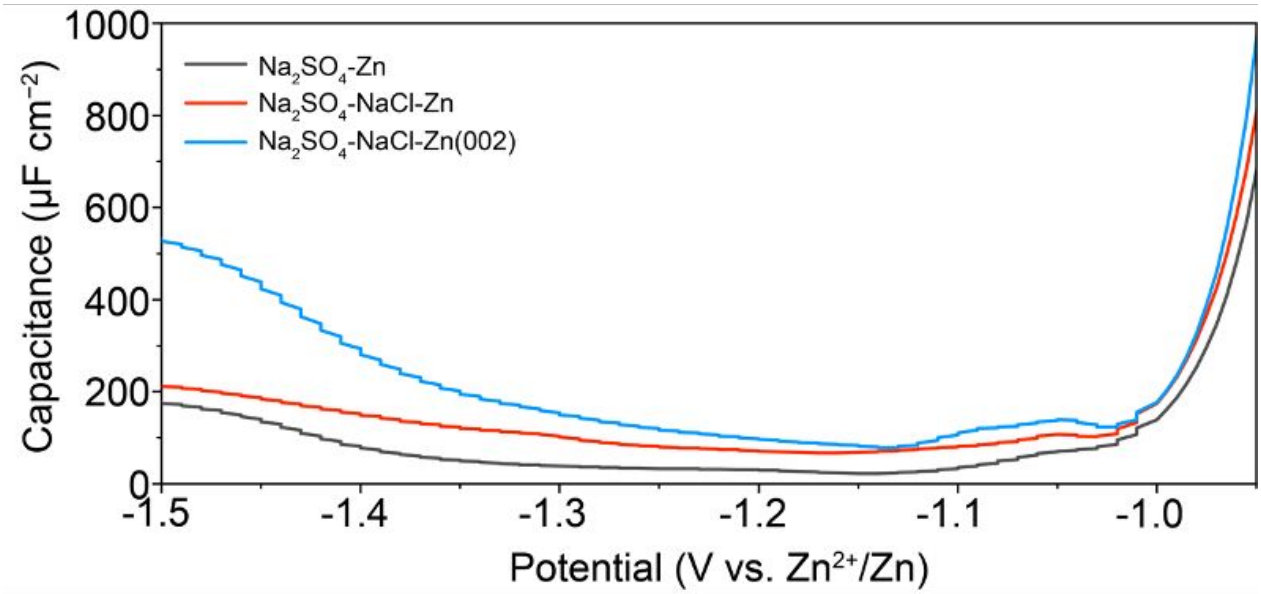

Figure S6. Differential capacitance curves of commercial Zn metal in $NaSO_4$-H_2O and $NaSO_4$-NaCl-H_2O electrolytes, and the differential capacitance curve of (002) crystal facet-oriented Zn metal in $NaSO_4$-NaCl-H_2O electrolyte.

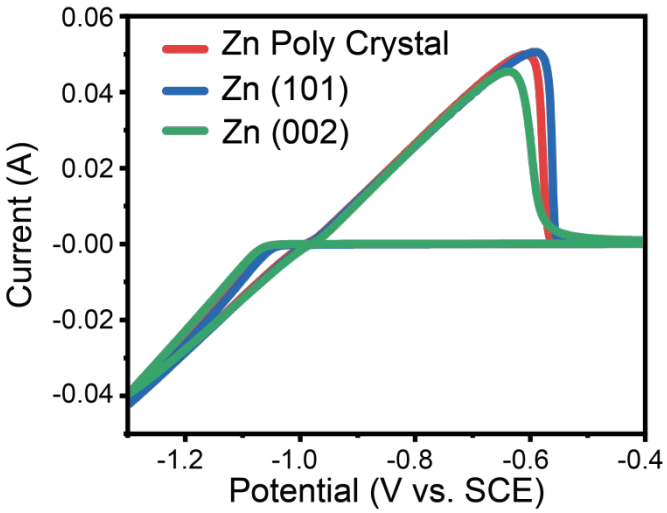

Figure S7. CV test of different Zn facets in a three-electrode system.

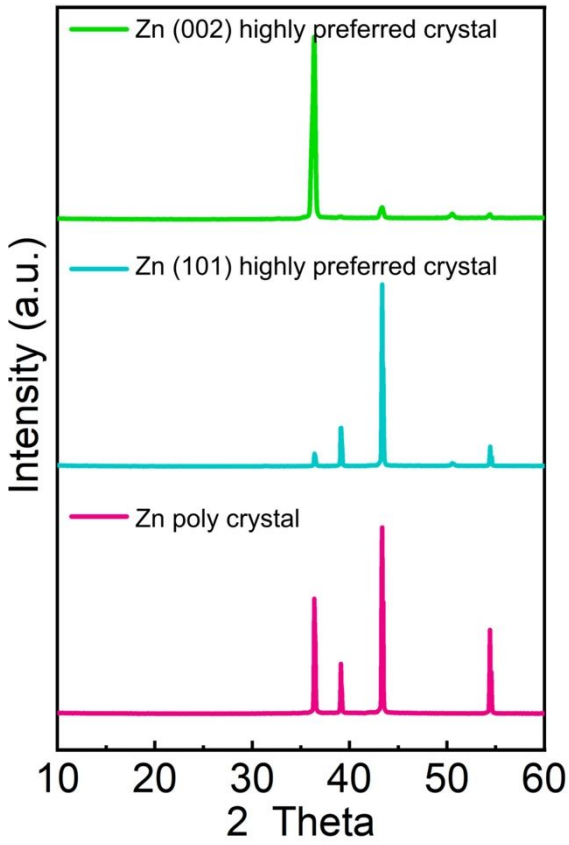

Figure S8. The XRD pattern of Zn polycrystal , Zn (101) highly preferred crystal and Zn (002) highly preferred crystal, respectively.

Method for preparing Zn electrode with (101) and (002) preferred orientation:

Preparation of electroplating solution: Initially, 250 mg of protein hydrolysate and 2 mol L^{-1} of $ZnSO_4$ were mixed in 2N sulfuric acid solution (1 L) under continuous stirring for 20 min at room temperature. Subsequently, a Zn plate was utilized as the working electrode, platinum as the counter electrode, and standard calomel electrode (SCE) as the reference electrode. The electrodes were immersed in the electroplating solution and subjected to constant potential electrodeposition at −1.2 V. Finally, the Zn electrode with (101) preferred orientation was obtained after washing thoroughly with DI water and drying at 70 °C for 24 h.

The Zn electrode with (002) preferred orientation was prepared using the same electroplating method in a $ZnSO_4$-CFTA-H_2O electroplating solution.

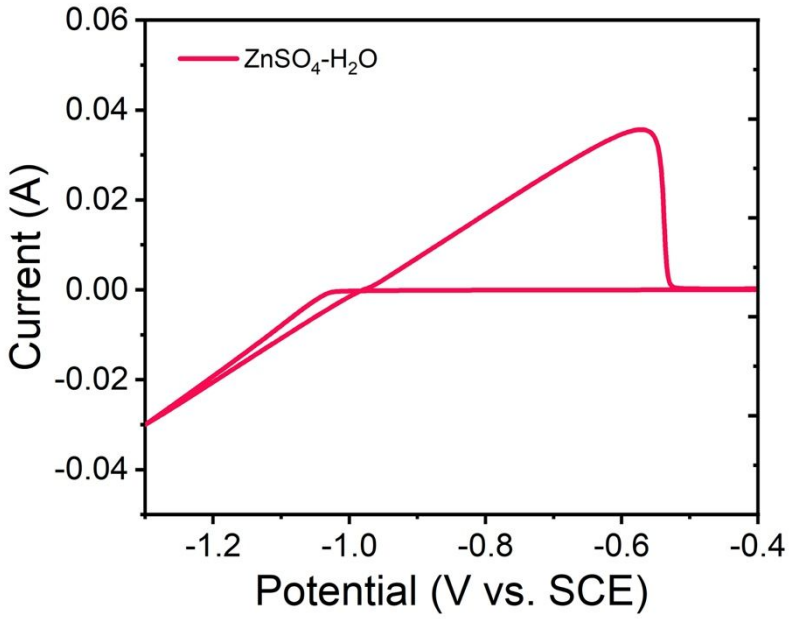

Figure S9. CV curve tested in a 3-electrode system, in which commercial Zn poly crystal is used as the working electrode and $ZnSO_4$ as the electrolyte.

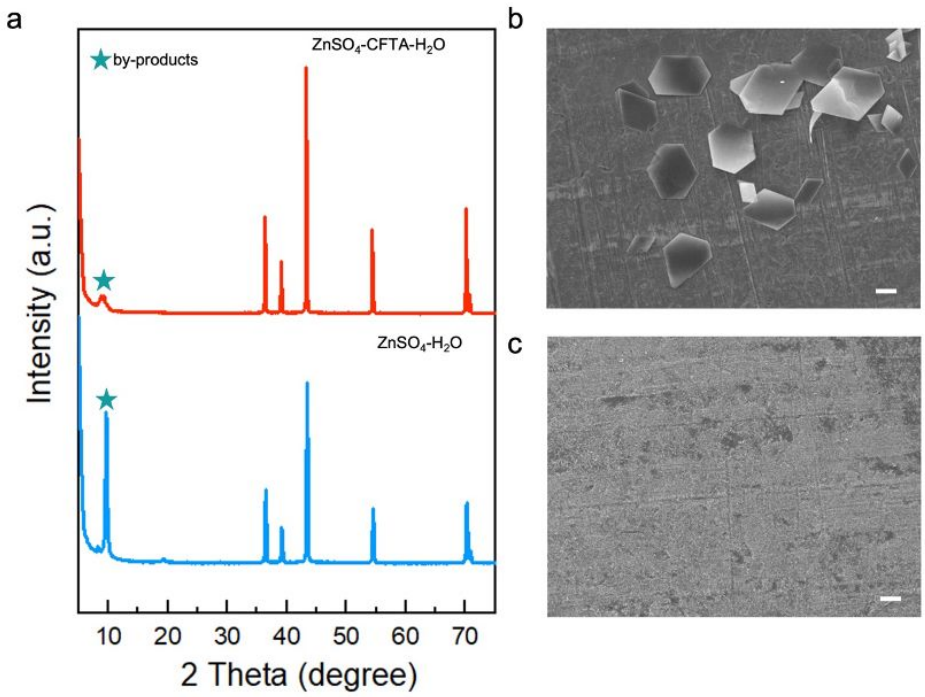

Figure S10. Characterization of the Zn metal after standing for 48 hours in n different aqueous electrolytes. a) XRD pattern of Zn in $ZnSO_4$-CFTA-H_2O and $ZnSO_4$-H_2O, respectively. b) SEM images of the Zn metal after standing for 48 hours in $ZnSO_4$-H_2O electrolyte. c) SEM images of the Zn metal after standing for 48 hours in $ZnSO_4$-CFTA-H_2O electrolyte. Scale bar: μm.

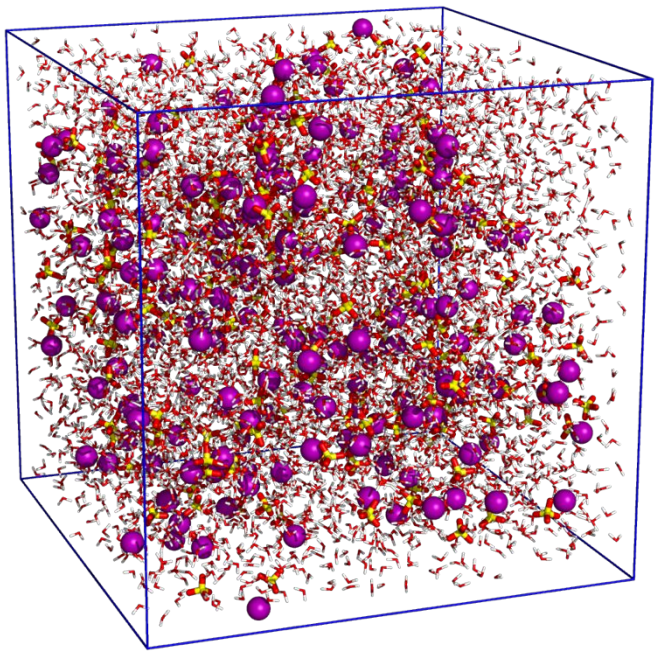

Figure S11. 3D snapshot of pure $ZnSO_4$ system obtained from MD simulations.

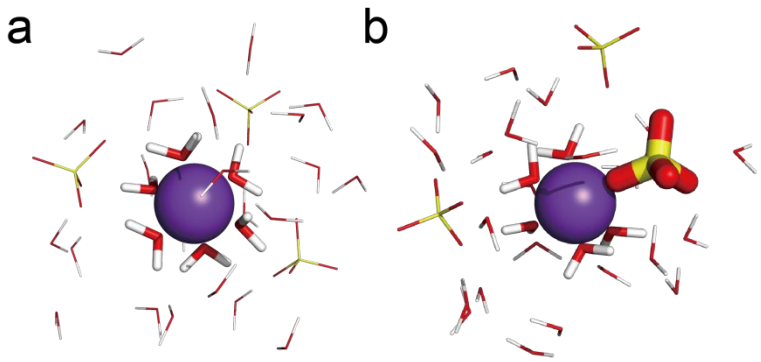

Figure S12. Zn^{2+} solvation structure originated from MD simulations in 2 M $ZnSO_4$ electrolyte.

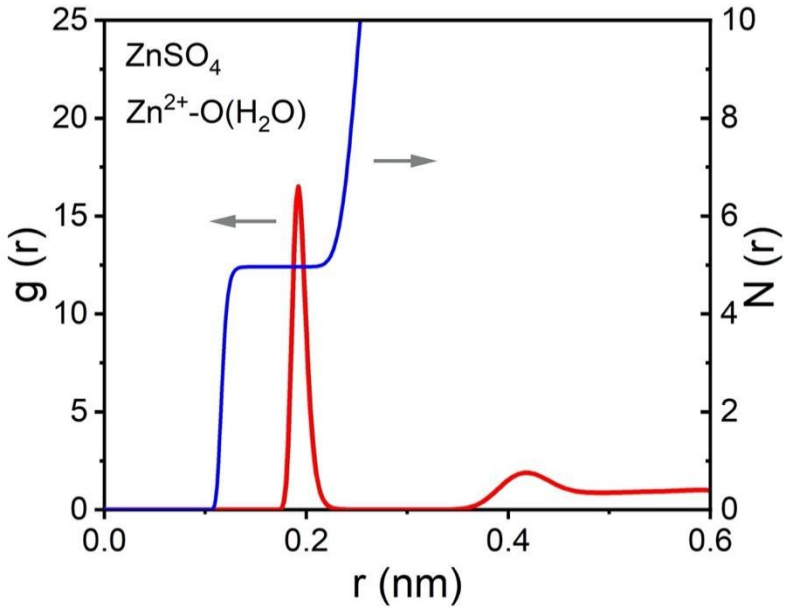

Figure S13. RDFs for Zn^{2+}-O (H_2O) collected from MD simulations in $ZnSO_4$- H_2O electrolyte.

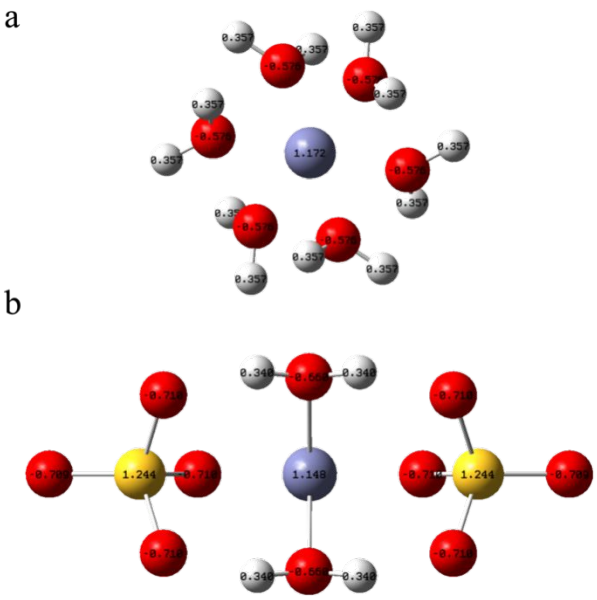

Figure S14. Electrostatic potential mapping of t (a) Zn^{2+}-$6H_2O$ and (b) Zn^{2+}-$2H_2O$-SO_4^{2-} solvation structures.

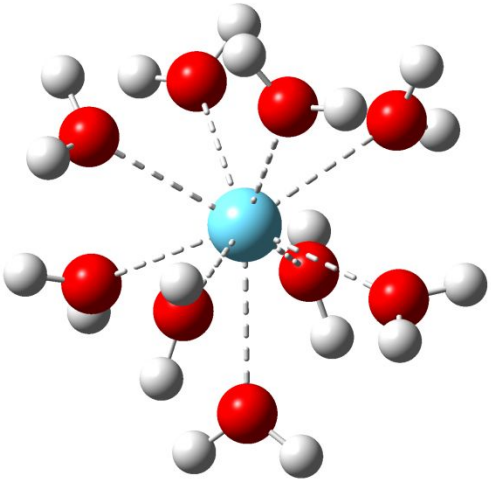

Figure S15. La^{3+} solvation structure with 9 H_2O molecules.

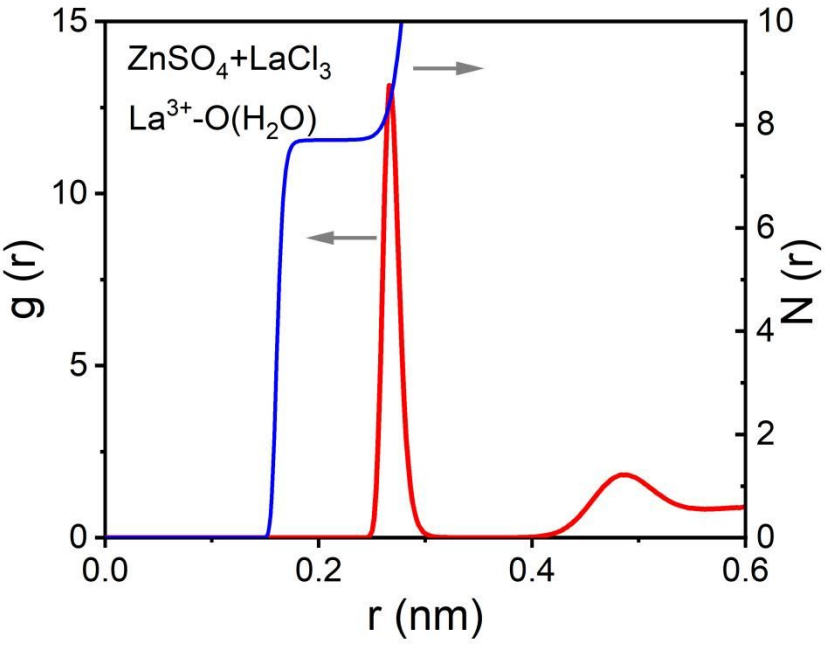

Figure S16. RDFs for La^{3+}-O (H_2O) collected from MD simulations in $ZnSO_4$-CFTA- H_2O electrolyte.

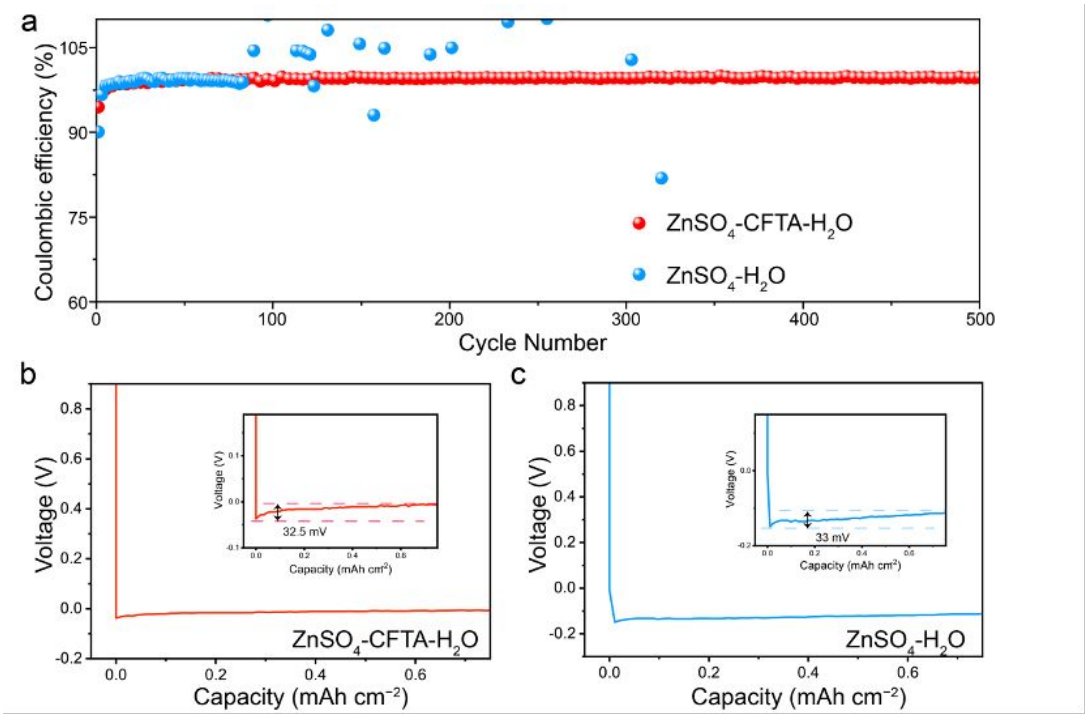

Figure S17. a) Zn plating/stripping Coulombic efficiency in different electrolytes at 5 mA cm^{-2} and 1 mAh cm^{-2}. b) Voltage-capacity curves deposited on the Zn electrodes in $ZnSO_4$-CFTA-H_2O electrolyte at a current density of 5mA cm^{-2}. c) Voltage-capacity curves deposited on the Zn electrodes in $ZnSO_4$-H_2O electrolyte at a current density of 5mA cm^{-2}.

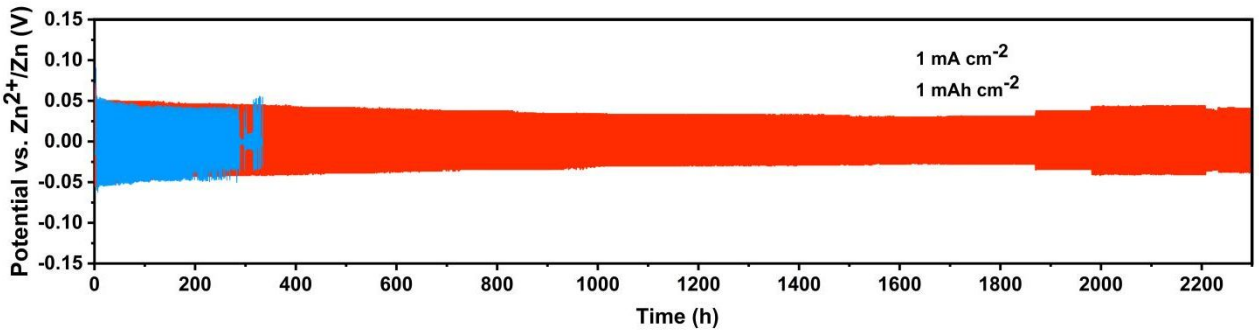

Figure S18. Long-term galvanostatic cycling performance of Zn||Zn symmetrical batteries using $ZnSO_4$-H_2O electrolyte and $ZnSO_4$-CFTA-H_2O electrolyte at 1 mA cm^{-2}, 1 mAh cm^{-2}.

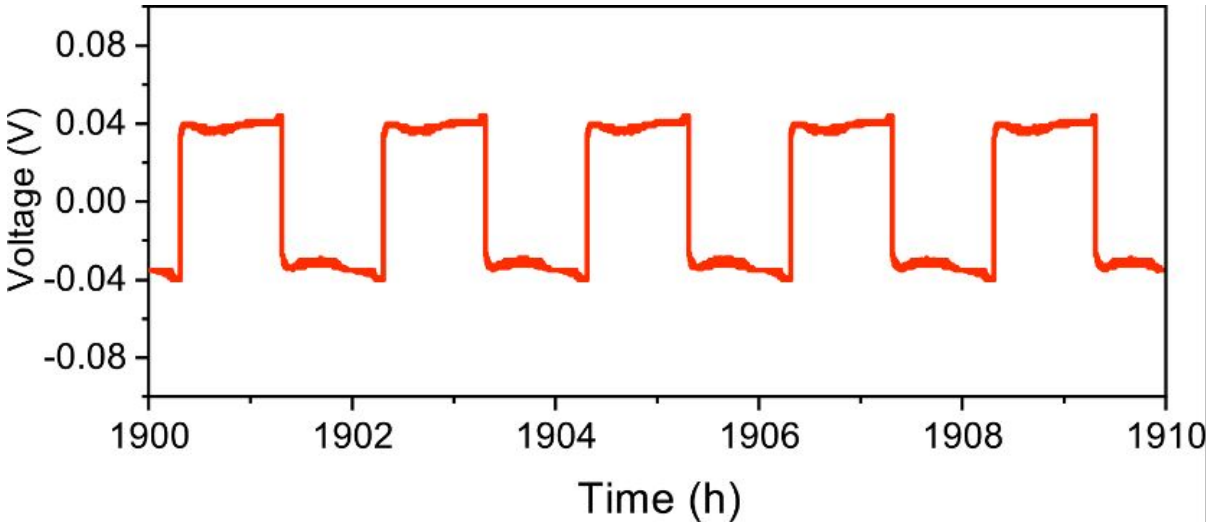

Figure S19. The performance for the 1900th to 1910th cycles of Zn||Zn symmetrical batteries using $ZnSO_4$-H_2O electrolyte and $ZnSO_4$-CFTA-H_2O electrolyte at 1 mA cm^{-2}, 1 mAh cm^{-2}.

The Zn||Zn symmetrical batteries using $ZnSO_4$-CFTA-H_2O electrolyte exhibited slight fluctuations in polarization voltage after 1900 cycles at 1 mA cm^{-2}, 1 mAh cm^{-2}. Therefore, we provided an enlarged graph of the 1900^{th}-to-1900^{th} cycles, showing normal charge-discharge curves, proving that the fluctuations were not caused by a soft short circuit. This may be due to temperature variations during the extended testing period.

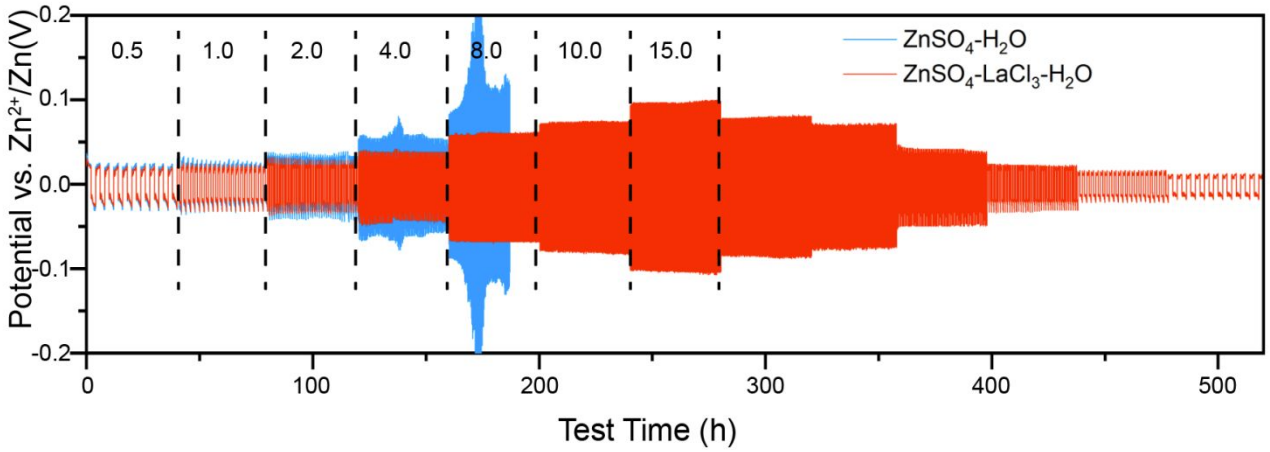

Figure S20. Rate performance of Zn||Zn symmetrical batteries using $ZnSO_4$-H_2O electrolyte and $ZnSO_4$-CFTA-H_2O electrolyte.

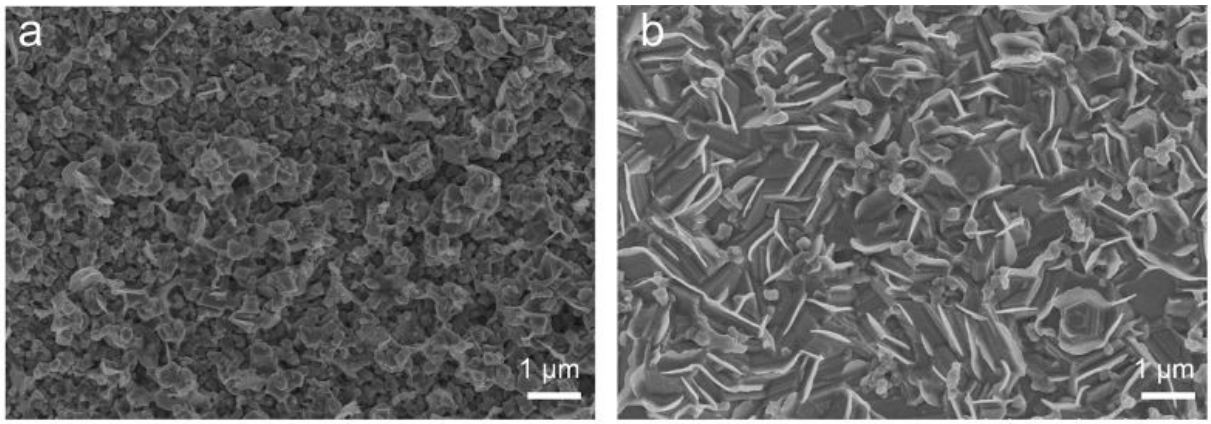

Figure S21. a) SEM images of the Zn electrodeposits in the $ZnSO_4$-$La(NO_3)_3$-H_2O electroplating solution at a current density of 5 mA cm^{-2}. b) SEM images of the Zn electrodeposits in the $ZnSO_4$-$ZnCl_2$-H_2O electroplating solution at a current density of 5 mA cm^{-2}.

To investigate which ion, La^{3+} or Cl^-, exerts a more significant influence on the nucleation behavior of Zn, we conducted experiments using $ZnCl_2$ and $La(NO_3)_3$ as additives, respectively. At a current density of 5 mA cm^{-2}, Zn deposition was performed on commercial Zn foil, and SEM was employed to characterize the Zn deposits, as illustrated in the Figure S21. The SEM results revealed that in the $ZnSO_4$-$La(NO_3)_3$-H_2O electroplating solution, the morphology of the Zn deposits was relatively smooth, showing small particles. This is likely attributed to the electrostatic shielding effect produced by La^{3+} at the tips of the Zn deposits. In contrast, the SEM characterization of the Zn deposits exhibited a vertically oriented growth morphology in the $ZnSO_4$-$ZnCl_2$-H_2O electroplating solution.

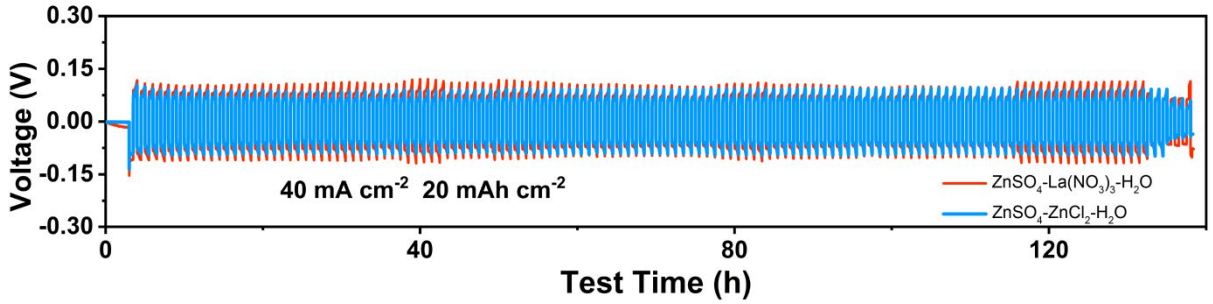

Figure S22. Long-term galvanostatic cycling performance of Zn||Zn symmetrical batteries using $ZnSO_4$-$La(NO_3)_3$-H_2O electrolyte and $ZnSO_4$-$ZnCl_2$-H_2O electrolyte.

Furthermore, we tested Zn||Zn symmetric cells at a current density of 40 mA cm^{-2}, 20 mAh cm^{-2} in Figure S22. Compared to cells with pure $ZnSO_4$ electrolyte, those with Cl^- or La^{3+} additives exhibited enhanced cycling performance, with both achieving approximately 130 h. In contrast, the Zn||Zn symmetric cells utilizing $ZnSO_4$-CFTA-H_2O electrolyte demonstrated a stable cycling performance of up to 300 h. This indicates that the individual addition of either Cl^- or La^{3+} can improve the performance of the battery to a certain extent, but this enhancement is limited. Therefore, it is only when Cl^- and La^{3+} synergistically interact that the preferential growth of the Zn (002) crystal facet can be effectively promoted, which is essential for optimizing battery performance.

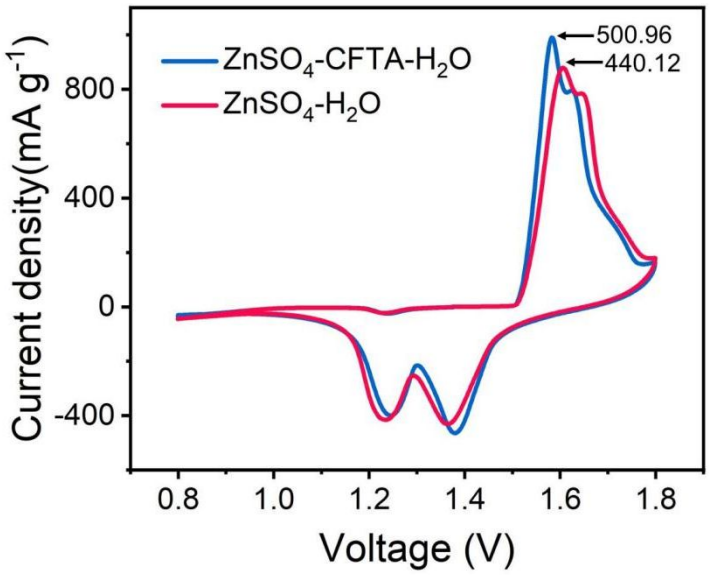

Figure 23. CV curves of Zn||MnO_2 cells at 0.2 mV s^{-1} in $ZnSO_4$-CFTA-H_2O electrolyte and $ZnSO_4$-H_2O electrolyte, respectively.